Polymer Chemistry

PAPER

View Article Online
View Journal | View Issue

Cite this: *Polym. Chem.*, 2017, **8**, 4528

Highly stable Au nanoparticles with double hydrophilic block copolymer templates: correlation between structure and stability†

Eunyong Seo,‡[a] Sang-Ho Lee,‡[b] Sangho Lee,[c] Soo-Hyung Choi,[c] Craig J. Hawker[b] and Byeong-Su Kim*[a,d]

Received 9th May 2017,
Accepted 4th July 2017

DOI: 10.1039/c7py00773f

rsc.li/polymers

We herein report a facile synthetic method for preparing gold nanoparticles (Au NPs) with superior colloidal stability using a series of double hydrophilic block copolymers (DHBC), poly(ethylene oxide)-*block*-poly(acrylic acid) (PEO-*b*-PAA), as a template (Au@DHBC NPs). Due to the presence of a well-defined polymeric shell around the Au NPs, this DHBC-based synthetic method provides superior stability when compared to conventional citrate-based synthesis. We have investigated NP performance by systematically varying the molecular weight of the interacting PAA block from 5000 g mol^{-1} to 27 000 g mol^{-1}. Interestingly, the size of the Au NPs did not significantly depend on the molecular weight of the PAA block and the density of DHBC present around a single NP decreased upon an increase in the molecular weight of the PAA block. Cyanide etching of Au@DHBC NPs further confirmed the presence of DHBC with different densities around the NPs, resulting in tunable stability. Considering the structural variability of DHBCs, it is expected that the approach presented in this study will offer a new means for creating Au NPs with enhanced colloidal stability for potential biological and biomedical applications.

Introduction

In the past few decades, tremendous effort has been devoted to designing nanomaterials with unique characteristics, different from those of bulk materials, through the controlled synthesis and functionalization of materials on a nanometre scale.[1–3] Colloidal gold nanoparticles (Au NPs) have been widely applied in the fields of biology and biomedicine as biological labels, visualizing reporters, and agents for thermal therapy.[4–8] Although NPs are more stable in the bulk phase, attempts at preserving and enhancing the nanoscale properties of Au NPs under biological environments such as varying the pH and ionic strengths have received significant attention allowing their successful utilization in a wider field of study.[9]

Typically, Au NPs of size ranging from a few to several hundreds of nanometers have been prepared by either adsorption or chemical binding of small molecules such as citric acid or thiol-functionalized chemical species that act as surfactants and stabilizers.[10,11] Despite the simple and successful synthesis of Au NPs by these methods, the stability of Au NPs is often limited in various biological environments.[12] Thus, an additional process such as the introduction of polymers is required for surface passivation of as-prepared NPs, whereby the colloidal stability is enhanced by strong inhibition of the non-specific adsorption of biomolecules such as peptides and proteins. In particular, water-solubilizing polymeric ligands (*e.g.*, poly(ethylene oxide) (PEO)) can not only interrupt undesired interactions with natural materials, but also provide an antifouling effect through the organization of the copolymers on the NP surface.[13–15]

As an alternative approach, a variety of block copolymers have been studied as highly attractive materials that can improve the stabilization of NPs.[16–18] Among them, double hydrophilic block copolymers (DHBCs) are known to facilitate the formation and controlled growth of such nanostructures as well as impart tunability due to the presence of chemically different functionalities of each block.[19–21] In particular, the direct utilization of DHBC as a template and a stabilizer in NP synthesis has recently been exemplified as an efficient alternative to either the conventional surfactant-based method or protocols involving post-functionalization with macromolecular ligands (Scheme 1). From a structural viewpoint, the DHBC template consists of two chemically distinct segments with

[a]*Department of Energy Engineering, Ulsan National Institute of Science and Technology (UNIST), Ulsan 44919, Korea. E-mail: bskim19@unist.ac.kr*
[b]*Materials Research Laboratory and Departments of Materials, Chemistry and Biochemistry, University of California, Santa Barbara, California 93106, USA*
[c]*Department of Chemical Engineering, Hongik University, Seoul 04066, Korea*
[d]*Department of Chemistry, Ulsan National Institute of Science and Technology (UNIST), Ulsan 44919, Korea*

†Electronic supplementary information (ESI) available. See DOI: 10.1039/c7py00773f

‡These authors contributed equally to this work.

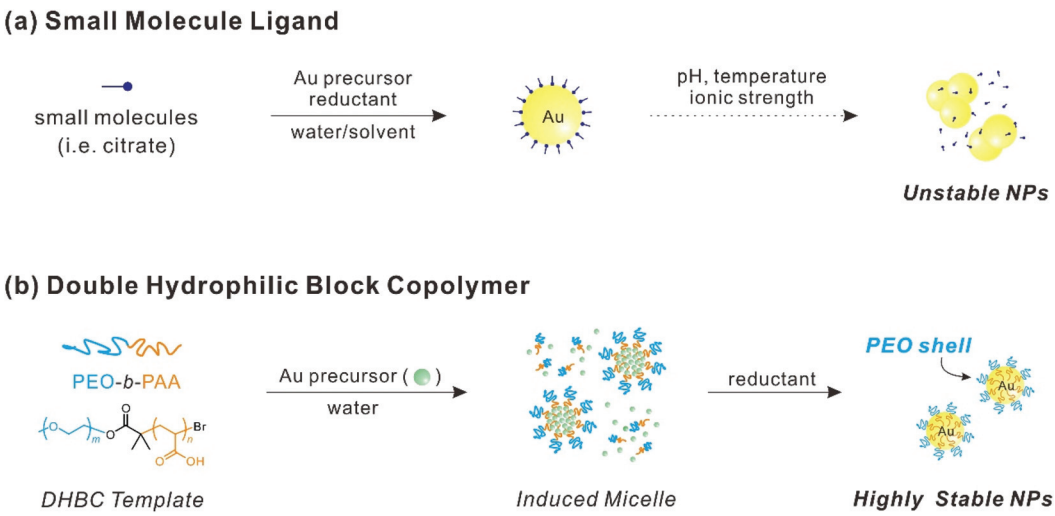

Scheme 1 Synthetic approaches to Au NPs *via* small molecules or DHBC templates and the corresponding stability under various conditions.

hydrophilic features, which act as the interacting and solvating block, respectively.[22,23] Generally, the interacting block in DHBC plays an important role in inducing polyionic complexation (PIC) with metal ions, which determines the structural properties of the corresponding metal NP. In contrast, the solvating block affects the solubility and stability of the resulting NPs by forming a protective shell on the surface.

In particular, the stability depends on the shell density, which can be tuned by controlling the number of solvating chains present on the surface of NPs.[24]

Despite previous efforts examining the synthesis of DHBC-based NPs, extending the application of these DHBCs is still challenging because micellization and the corresponding mineralization during the growth of NPs are highly dependent on various factors.[25–28] For example, internal parameters such as the nature of the respective blocks utilized, the molecular weight of polymers, and the ratio of reactants to polymers, along with external factors such as the pH, temperature, ionic strength, and specific complexation in solution, all play a critical role in the synthesis and subsequent properties of the NP.

In order to overcome these challenges, a poly(ethylene oxide)-*block*-poly(acrylic acid) (PEO-*b*-PAA; PEO: solvating block for NP, PAA: interacting block for Au precursor) block copolymer was designed and its effect on the formation and the corresponding stability of Au NPs was studied. In particular, a series of PEO-*b*-PAA based DHBC templates were synthesized using the PEO-Br macroinitiator and Cu-based atom transfer radical polymerization (ATRP) (PAA blocks ranging from 5000 g mol^{-1} to 27 000 g mol^{-1}). It is known that the DHBC template can form a micellar structure in solution by complexation of the carboxylate groups present in the interacting PAA block with the starting Au precursor salts.[29] Subsequently, these micellar aggregates can be transformed into Au NPs by reaction with a reducing agent. As an additional benefit, the well-defined PEO shell block provides stability to the NPs from external conditions (Scheme 1b).

The aim of this study is therefore to synthesize highly stable Au NPs using DHBC templates and to determine the correlation between the number of interacting blocks present on the DHBC template and the structural properties of NPs and the corresponding stability of the synthesized NPs. Significantly, multiple functionalities can be introduced using DHBC, as each block in the DHBC is highly tunable in terms of molecular weight and structural control. For this reason, the synthetic approach of utilizing DHBC as a template provides a facile means for preparing tunable NPs with increased stability.

Experimental

Materials

Poly(ethylene oxide) (PEO, M_n = 5000 g mol^{-1}), *N*,*N*,*N*′,*N*″,*N*″-pentamethyl diethylenetriamine (PMDETA), 2-bromoisobutyryl bromide, and trifluoroacetic acid (TFA) were purchased from Sigma-Aldrich and used as received. The monomer *tert*-butyl acrylate (*t*BA, Aldrich, purity >99%) was passed through a plug of basic alumina to remove the inhibitors before use. Toluene was dried and purified by passing through purification columns (Solvent Dispensing System, Glass Contour) and dry nitrogen was bubbled through the solvent for 15 min immediately before use. Gold(III) chloride trihydrate ($HAuCl_4 \cdot 3H_2O$) and L-ascorbic acid were obtained from Sigma-Aldrich, and sodium hydroxide was purchased from Junsei Chemical Co. All these were used without further purification.

Synthesis of the PEO-Br macroinitiator

5.0 g (0.10 mol) of α-methoxy-ω-hydroxy poly(ethylene oxide) (MeO-PEO-OH, M_n = 5000) was added to 30 mL of anhydrous THF and the flask was cooled to 0 °C using an ice-bath. 2-Bromoisobutyryl bromide was added slowly into the reaction flask over 1 h *via* a syringe pump with constant pressure. The reaction solution was gradually warmed to room temperature

and stirred overnight. Subsequently, the solvent was removed on a rotary evaporator and the residue was dissolved in water. The mixture was extracted with dichloromethane (DCM) and the organic extracts were dried over magnesium sulfate. The solution was filtered and concentrated using a rotary evaporator. The crude product was precipitated in diethyl ether and filtered three times to obtain the pure macroinitiator (4.7 g, 91% yield). ^{1}H NMR (600 MHz, $CDCl_3$, 298 K, ppm): δ 1.9 (6H, s, OCOC(CH_3)$_2$Br), 3.4 (3H, s, $CH_3OCH_2CH_2$–), 3.6 (456H, br s, –OCH_2CH_2–), 4.4 (2H, t, –CH_2CH_2OCOC(CH_3)$_2$Br).

General polymerization procedure

Polymerization was carried out by the syringe technique under dry argon in baked glass tubes equipped with a three-way stopcock or in sealed glass vials. A typical procedure for *tert*-butyl acrylate (*t*BA) with PEO-Br/CuBr/PMDETA is given. For PEO_{5k}-*b*-P*t*BA_{12k}, in a round-bottom flask (50.0 mL) filled with argon was placed CuBr (43.0 mg, 0.30 mmol), toluene (2.40 mL), *t*BA (3.50 mL, 24.0 mmol), PMDETA (0.75 mL, 0.30 mmol) and PEO-Br (1.03 g, 0.20 mmol) sequentially; the total volume was 6.65 mL. Immediately after mixing, aliquots (0.50–1.0 mL each) of the solution were injected into baked glass tubes, which were then sealed (except when a stopcock was used) and placed in an oil bath kept at 80 °C. After 4.5 h, the polymerization mixture was terminated by cooling to −78 °C in dry ice–methanol. Monomer conversion was determined from the residual monomer concentration measured by ^{1}H NMR spectroscopy (80% conversion) and the obtained polymer was purified by passing through basic alumina to remove the Cu catalyst. The final product was precipitated in cold hexane and dried overnight under vacuum at room temperature ($M_{n,\ SEC}$ = 18 000 g mol^{-1}, M_w/M_n = 1.11).

General procedure for hydrolysis

In a round-bottom flask, PEO_{5k}-*b*-P*t*BA_{12k} ($M_{n,\ SEC}$ = 18 000 g mol^{-1}, M_w/M_n = 1.11) was dissolved in 5 mL of DCM and 5 mL of TFA was slowly added into the flask at 0 °C. The solution was stirred overnight at room temperature. After hydrolysis was complete, the solvent was removed *via* rotary evaporation. The crude product was dissolved in THF and dialyzed against deionized water to remove the reactant residues. The pure white product PEO-*b*-PAA was obtained by freeze-drying (1.5 g, 53% yield). ^{1}H NMR (600 MHz, D_2O, 298 K, ppm): δ 1.1 (6H, t, OCOC(CH_3)$_2$), 1.5 (192H, s, CH_2CHCOOH), 2.3 (96H, br s, CH_2CHCOOH), 3.2 (3H, s, $CH_3OCH_2CH_2$–), 3.5 (456H, br s –OCH_2CH_2–), 4.1 (2H, br s, –CH_2CH_2OCOC(CH_3)$_2$–).

General procedure for the synthesis of Au NPs using the PEO-*b*-PAA DHBC template

Au NPs with a double hydrophilic block copolymer shell (Au@DHBC NPs) were prepared according to the following protocol. First, PEO_{5k}-*b*-PAA_{7k} (24.8 mg, 0.20 mmol of carboxylic acid groups in the PAA block) was dissolved in 50 mL of deionized water, followed by the addition of 0.10 mL of 4.0 M NaOH (0.40 mmol, 2 equiv. for each carboxylic acid group in the PAA block). To this solution, $HAuCl_4{\cdot}3H_2O$ (26.2 mg, 0.067 mmol) was added and stirred for 5 min. Subsequently, 2 mL of 1 M ascorbic acid (2.0 mmol) was added and after 3 minutes of vigorous stirring, the solution underwent a color change to transparent red. After the reaction, the solution was dialyzed against deionized water using a dialysis membrane (MWCO 12 000–14 000, SpectraPore) to remove any residuals. The prepared suspension of Au@DHBC NPs exhibited good colloidal stability, lasting for more than six months without any precipitation.

Thermal stability and polymer composite of Au NPs

1.5 mL of Au@citrate and Au@PEO_{5k}-*b*-PAA_{7k} NP solutions (1.0 nM) was added separately to vials of 4 mL capacity and placed in a vacuum oven at 95 °C. These samples were removed from the oven at specific intervals, and cooled to room temperature to measure their absorbance using a UV-Vis spectrophotometer. A composite of Au NPs was prepared with the polymer gel matrix using agarose. For this purpose, 0.5 g of agarose powder was dissolved in 50 mL of water and this solution was gently shaken after heating for a minute in a microwave. The agarose solution was removed from the microwave after additional heating for 30 s. During the cooling down process, Au@citrate and Au@PEO_{5k}-*b*-PAA_{7k} NPs were added into the gel matrix at a specific temperature to form the polymer–NP composite. The final concentration of Au NPs in agarose gels was set at 0.10 nM.

Stability of Au NPs in various buffers

Stock solutions of several buffer such as MES buffer (50 mM, pH 6.0), phosphate buffers (100 mM, pH 7 and 8), and carbonate buffer (25 mM, pH 10.5) were prepared. Typically, 1 mL of the Au@citrate and Au@PEO_{5k}-*b*-PAA_{7k} NP solutions (1.0 nM) were dialyzed against 1 mL of the respective buffer solutions. The total volume and the final concentration of Au NPs in buffers were 2 mL and 0.5 nM, respectively. The absorbance and photographic images of each Au solution were obtained after 24 h to compare their colloidal stability in buffers.

Etching of Au NPs by cyanide ions

KCN solution (24 mM), and Au@citrate and Au@DHBC NP solutions (2 nM of each) were prepared separately. 1 mL of the KCN solution was added to 1 mL of the solution of Au NPs at room temperature. The absorbance of the mixtures was measured using a UV-Vis spectrophotometer at 520 nm at specific time intervals.

Measurements

^{1}H NMR spectra were recorded on a Varian 600 MHz instrument, and have been reported in parts per million (ppm). The signals for all polymers were measured relative to the residual solvent signals in $CDCl_3$ (7.26 ppm) or D_2O (4.79 ppm). Size-exclusion chromatography (SEC) traces and the polydispersity index (PDI) of polymers were measured using a Waters Alliance HPLC system equipped with a Waters 2414 refractive index detector using either a mixture of chloroform and trimethylamine or that of dimethylformamide (DMF) and LiBr. Poly(methyl methacrylate) (PMMA) homopolymers were used as standards for calibration. The as-synthesized copolymers

are denoted by PEO_{5k}-*b*-PAA_m, where *m* was calculated on the basis of degree of polymerization of *tert*-butyl acrylate ($DP_{n,\ tBA}$) in the PEO-*b*-P*t*BA copolymer, which was determined by ^{1}H NMR. The morphology, size, and size distribution of the prepared NPs were investigated using transmission electron microscopy (TEM) (Tecnai FEI T20 and JEOL JEM-2100, an accelerating voltage of 200 kV, Gatan CCD camera). UV-Vis spectra were recorded using a UV-Vis spectrophotometer (Shimadzu). The size distribution analyses were performed using dynamic light scattering (a Wyatt Technology DynaPro NanoStar instrument and a Nano Particle Analyzer) using a photon source with a wavelength of 532 nm for micelles and 662 nm for NPs. The temperature was fixed at 25 °C and the data were analyzed by the cumulant fitting method.

Results and discussion

Syntheses and characterization of PEO-*b*-PAA DHBC templates

In order to study the effect of the PAA block structure on the formation of Au NPs and their corresponding colloidal stability, a series of PEO-*b*-P*t*BA copolymers were prepared from the PEO macroinitiator PEO-Br (M_n = 5000) *via* Cu-based ATRP in conjunction with PMDETA as a ligand at 80 °C in toluene. Five PEO-*b*-P*t*BA copolymers were successfully prepared with narrow molecular weight distributions (M_w/M_n < 1.2; Table 1 and see Fig. S1 in the ESI†) and analyzed by ^{1}H NMR spectroscopy. For example, the PEO_{5k}-*b*-$PtBA_{12k}$ (Fig. 1 and entry P2 in Table 1) shows characteristic peaks for the methyl group at the chain end of the PEO block (*a*, 3H) and for the *tert*-butyl groups of the P*t*BA block (*g*, 9H). Peak integration leads to a degree of polymerization of *t*BA ($DP_{n,\ tBA}$ = 96) and a total molecular weight of PEO_{5k}-*b*-$PtBA_{12k}$ ($M_{n,\ NMR}$ = 17 400).

The different copolymer samples were then treated with trifluoroacetic acid (TFA) in DCM overnight at room temperature, leading to the deprotection of the *tert*-butyl groups on the P*t*BA chain. Subsequently, all samples were purified by dialysis in water for several days with the final structure of the PEO-*b*-PAA copolymers being confirmed by ^{1}H NMR.

For example, the peak for the *tert*-butyl group of PEO_{5k}-*b*-$PtBA_{12k}$ (*g*, 9H in Fig. 1b) disappeared after hydrolysis (Fig. 1c),

Table 1 Characteristics of all the polymers synthesized in this study[a]

		PEO-*b*-P*t*BA					PEO-*b*-PAA
Entry	Composition	$DP_{n,\ EO}$[g]	$DP_{n,\ tBA}$[g]	$M_{n,\ SEC}$[h]	M_w/M_n[h]	$M_{n,\ NMR}$[g]	$M_{n,\ NMR}$[g]
P1[b]	PEO_{5k}-*b*-$PtBA_{8k}$	114	62	16 300	1.09	13 100	9600
P2[c]	PEO_{5k}-*b*-$PtBA_{12k}$	114	96	18 000	1.11	17 400	12 100
P3[d]	PEO_{5k}-*b*-$PtBA_{20k}$	114	157	23 000	1.16	25 300	16 500
P4[e]	PEO_{5k}-*b*-$PtBA_{30k}$	114	235	34 800	1.12	35 300	22 100
P5[f]	PEO_{5k}-*b*-$PtBA_{47k}$	114	368	48 100	1.16	52 300	31 700

[a] All polymerizations were performed in toluene at 80 °C. [b] $[tBA]_0/[PEO\text{-}Br]_0/[CuBr]_0/[PMDETA]_0$ = 2850/30/45/45 mM. [c] $[tBA]_0/[PEO\text{-}Br]_0/[CuBr]_0/[PMDETA]_0$ = 3600/30/45/45 mM. [d] $[tBA]_0/[PEO\text{-}Br]_0/[CuBr]_0/[PMDETA]_0$ = 5700/30/45/45 mM. [e] $[tBA]_0/[PEO\text{-}Br]_0/[CuBr]_0/[PMDETA]_0$ = 3500/12/36/36 mM. [f] $[tBA]_0/[PEO\text{-}Br]_0/[CuBr]_0/[PMDETA]_0$ = 4300/10/30/30 mM. [g] The degrees of polymerization (DP_n) of PEO and P*t*BA were calculated by ^{1}H NMR. [h] The number-averaged molecular weight (M_n) and molecular weight distribution (M_w/M_n) of PEO-*b*-P*t*BA copolymers were determined by size-exclusion chromatography (SEC) using PMMA as a standard for calibration.

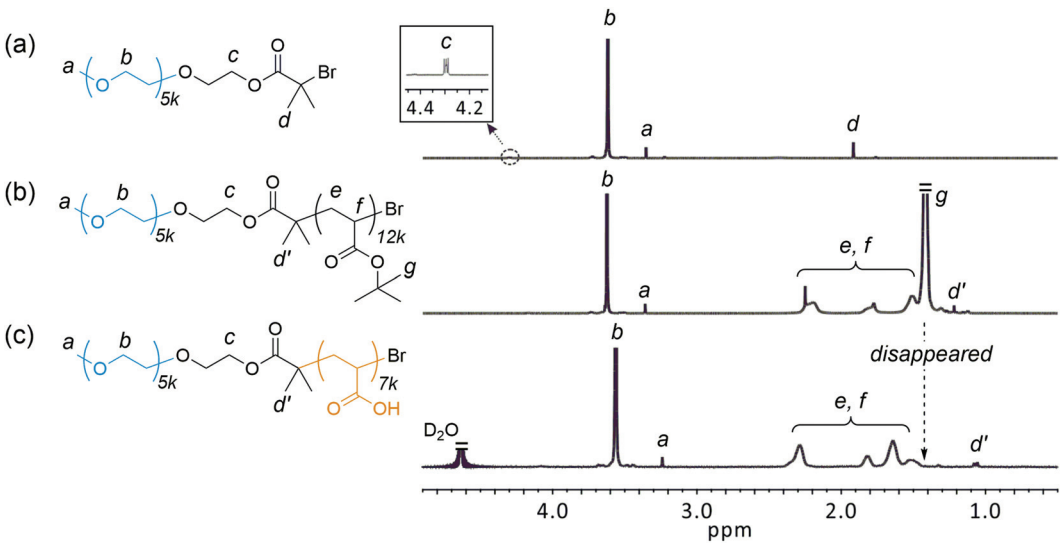

Fig. 1 ^{1}H NMR spectra of (a) PEO-Br macroinitiator in $CDCl_3$, (b) PEO_{5k}-*b*-$PtBA_{12k}$ copolymer in $CDCl_3$, and (c) PEO_{5k}-*b*-PAA_{7k} in D_2O.

indicating that the *tert*-butyl groups of the P*t*BA block were fully deprotected.

Influence of the stoichiometry of the interacting block and the Au precursor on the synthesis of Au NPs

It is important to understand the relationship between the interacting PAA block of the PEO-*b*-PAA template and the Au precursor ($HAuCl_4$) as the carboxylate group is a primary contributor to controlling the growth of the Au NPs. In general, the evaluation of quantitative interactions between the interacting PAA block and metal ions is rather challenging by conventional spectroscopic tools such as ^{1}H NMR due to broad and insignificant peak changes. Therefore, sodium acetate was employed as a model compound instead of the PAA block to evaluate the association using ^{1}H NMR (Fig. 2). For example, on mixing sodium acetate and $HAuCl_4$ in methanol-d_4 at room temperature, the peak corresponding to the methyl group in sodium acetate shifted downfield, indicating that the acetate ion interacts with the Au ions (Fig. 2a). The stoichiometry was estimated to be 2 : 1 (one metal ion per two acetate molecules) by a Job's plot based on the chemical shift change of the acetate proton (peak *a*) and the molar fraction of acetate units (χ): [NaOAc]/[$HAuCl_4$] = 1/0–0/1, [NaOAc] + [$HAuCl_4$] = 10.0 mM (Fig. 2b).

Based on this association behaviour, the relationship between the micellar structures and the corresponding NPs from the synthetic polymer template at varying molar ratios (R, [AA in DHBC template]/[$HAuCl_4$] = 0.5–4.0) was also investigated by DLS and TEM analysis (Fig. 3 and Table S1†). For example, PEO_{5k}-*b*-PAA_{7k} (entry P2 in Table 1) was used to study the effect of the molar ratio of interacting units (the carboxylate group in the PAA block) and $HAuCl_4$ for the formation of micelles and the corresponding Au NPs. The size of micelles progressively became larger as the amount of the DHBC template increased to a defined molar ratio ($R \leq 1.5$). This observation suggested that the number of interacting units in the DHBC template were insufficient for complete coordination with Au precursor ions (Fig. 3a). Moreover, the uncoordinated Au ions in solution randomly participated in the formation of Au NPs, leading to uncontrolled NP clusters when a small amount of DHBC was used (Fig. 3b). These results indicated that the size of micelles depends on the amount of Au ions coordinated to the DHBC template and the ratio of the interacting units and the Au precursor is critical in order to control the structure of the resulting Au NPs.

In addition, TEM analyses provided details of the optimum molar ratio required for a controlled synthesis of Au NPs. As the R value increased, the structure of the Au NPs became homogeneous, and their size gradually decreased. When the R

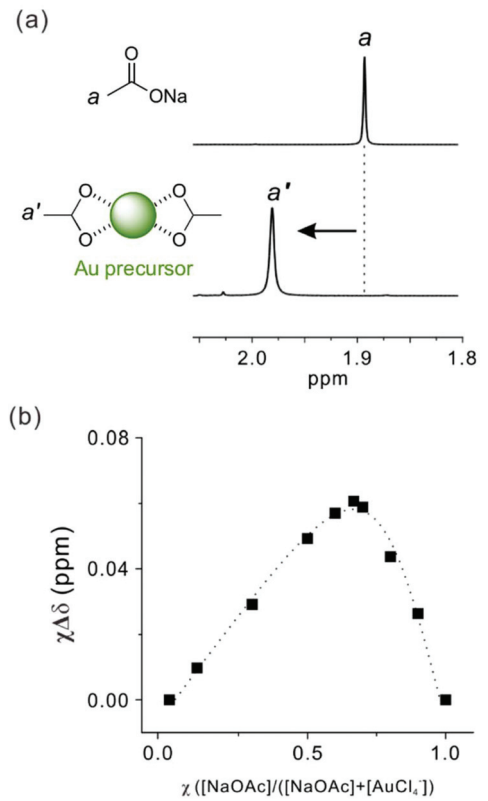

Fig. 2 (a) ^{1}H NMR spectra of sodium acetate (top) and a 2 : 1 mixture of sodium acetate and the Au precursor (bottom) in methanol-d_4 at room temperature. (b) Job's plot of the association of sodium acetate with the gold precursor ($HAuCl_4$) determined from the change in chemical shift (ppm) of NMR peak *a*. χ was defined as the molar ratio of sodium acetate to the total amount of sodium acetate and the Au precursor. The plot showed a maximum at χ = 0.667.

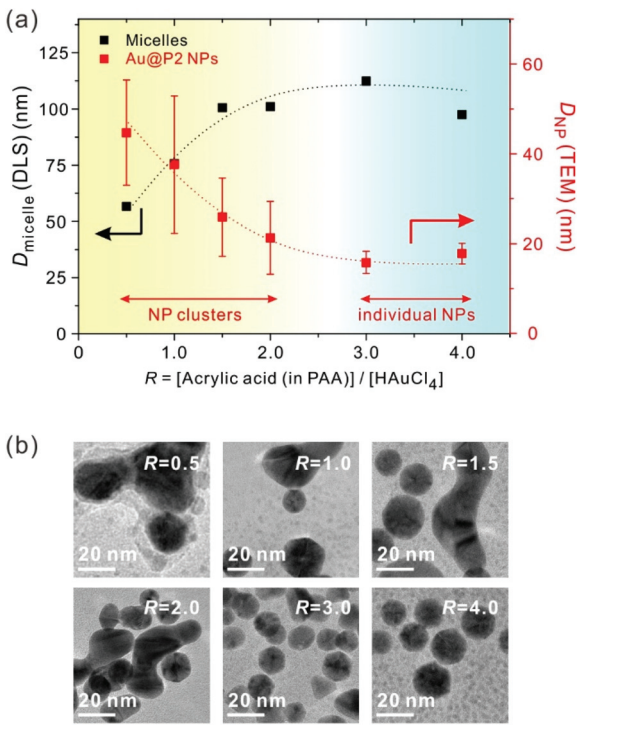

Fig. 3 (a) DLS and TEM analyses of micelles (before reduction) and the corresponding Au NPs (after reduction) prepared from PEO_{5k}-*b*-PAA_{7k} and $HAuCl_4$ with varying molar ratios (R = 0.5–4.0). (b) A series of TEM images of Au NPs prepared at a specific R value.

value reached 3, only individual Au NPs were found to be observed in solution. This observation indicated that the Au ions were fully coordinated with the DHBC template and well-defined micellar structures were present in the system. The discrepancy in the coordination number required for the DHBC template (R = 3) and the model compound (R = 2) is likely due to the steric hindrance and repulsion of carboxylate groups along the PAA backbone, leading to a decrease in the association ability between the interacting unit and the Au precursor ion. Therefore, the molar ratio of interacting units and Au precursor was optimized as R = 3 for the DHBC system during the controlled synthesis of Au NPs.

Effect of the DHBC template on the Au NP surface

As discussed in the previous section, the interacting PAA block of the PEO-*b*-PAA DHBC template influences the formation of Au NPs. The covalently bonded solvating PEO block, on the other hand, is located on the surface of the Au NPs with these PEO blocks acting as a protective shell on the surface of the Au NPs. The stability of Au NPs prepared using the PEO_{5k}-*b*-PAA_{7k} template (Au@P2 in Table 2) was then evaluated under thermal conditions and in the presence of biological buffers.

Table 2 Characterization of Au NPs prepared using citrate and DHBC templates[a]

Entry	Ligand for NP synthesis	D_{NP}[b] (nm) (TEM)	D_h[c] (nm) (DLS)
Au@citrate	Citric acid	17.1 ± 1.2	n.d.
Au@P1	PEO_{5k}-*b*-PAA_{5k}	17.3 ± 3.1	31.6
Au@P2	PEO_{5k}-*b*-PAA_{7k}	16.7 ± 3.3	26.2
Au@P3	PEO_{5k}-*b*-PAA_{11k}	19.2 ± 3.8	27.6
Au@P4	PEO_{5k}-*b*-PAA_{17k}	15.8 ± 3.0	29.4
Au@P5	PEO_{5k}-*b*-PAA_{27k}	16.3 ± 3.5	31.6

[a] All Au@DHBC NPs were synthesized with a fixed molar ratio (R = 3) of interacting units, carboxylate groups of PAA blocks, and Au precursors. [b] The diameter of Au NPs is denoted by D_{NP}, which was calculated by analyzing more than 100 Au NPs observed by TEM. [c] Average size of micelles is denoted by D_h, which was evaluated from the results of three measurements by DLS.

Conventional Au NPs prepared by the citrate reduction process were treated as a control (Au@citrate in Table 2). The stability of these NPs was evaluated by UV-Vis spectroscopy and TEM analyses (Fig. 4).

The thermal stability of Au@P2 and Au@citrate was first examined by incubation at 95 °C in aqueous medium (Fig. 4a). The color and absorbance of Au@P2 solution did not change over 24 h and the particle size and shape were also unchanged in TEM images, indicating that the Au@P2 was stable with no detectable aggregation at high temperatures. In clear contrast, the red color of Au@citrate quickly faded within 1 h at 95 °C with concomitant disappearance of the characteristic surface plasmon band. This phenomenon was further verified by TEM studies showing aggregated Au NPs.

Inspired by the increased thermal stability of Au@P2, a composite hydrogel containing Au NPs with agarose gel was also prepared (Fig. S2†). Both Au@P2 and Au@citrate aqueous solutions were added to the agarose solution at high temperature and then cooled to room temperature to form a hydrogel complex with Au NPs. While the Au@P2 NPs were well dispersed in the agarose gel matrix, the Au@citrate NPs showed a color change due to their instability under the high temperature conditions employed during the preparation of the hydrogel matrix.

The superior stability of Au@DHBC NPs was further evaluated under various pH and buffer conditions, including phosphate, MES, and carbonate buffers. The Au@P2 suspension shows high stability under acidic conditions (Fig. 4b) and in the presence of various buffers (Fig. 4c). In contrast, the stability of Au@citrate was significantly diminished under identical conditions due to interparticle coupling and/or NP ionization. These results highlight the significant influence of the PEO shell in enhancing Au NP stability.

Influence of DHBC template composition on the Au NPs and their stabilities

Five copolymers carrying different chain lengths of the PAA block but having identical PEO chain lengths were then

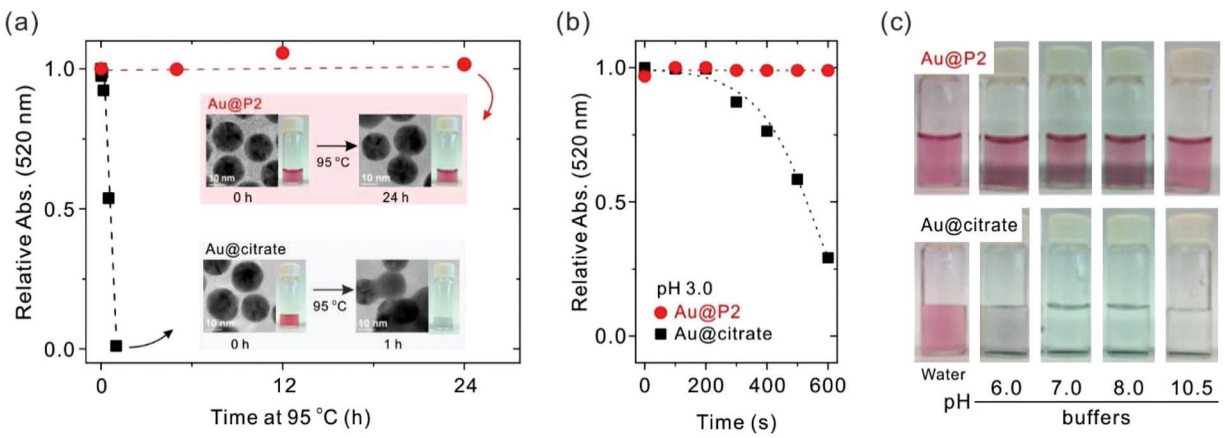

Fig. 4 (a) Thermal stability of Au NPs in water at 95 °C ([Au NP] = 1.0 nM). Stability of Au NPs (b) under acidic conditions (HCl solution, pH 3.0) and (c) in buffer solutions after incubation for 24 h (MES buffer, pH 6.0; phosphate buffers, pH 7.0 and 8.0; carbonate buffer, pH 10.5).

employed to investigate the effect of DHBC structures on the synthesis of Au NPs (Table 2). Using these DHBC templates, all Au NPs were prepared with a fixed molar ratio of the interacting unit, the carboxylate group of the PAA block, and the Au precursor (R = 3). The conversion of the Au precursor into metallic Au was estimated to be over 80%, confirmed using an ICP-OES instrument. Thus, considering a similar weight percentage of Au and DHBC before and after the synthesis of NP, we postulate that over 77% of the polymers are actually recovered during the synthesis (Table S2†). The size and shape of the NPs were determined by DLS analysis and from TEM images. The hydrodynamic diameter (D_h) determined from DLS measurements was relatively larger than that measured from TEM images, which supported the assertion that a thin polymeric layer surrounded the Au NPs.[23]

Interestingly, TEM images showed that the synthesized Au NPs had nearly similar sizes in the range of 16.3 to 19.2 nm (Table 2 and Fig. S3†), even though the molecular weight of PAA blocks in the DHBC templates was quite different (Table 2). It may be concluded that the molecular weight of the interacting block in DHBC is not a critical factor in determining the size of NPs. Recently, the Urban group has reported that the sizes of NPs were not influenced by changing the molecular weight of poly(methyl methacrylate) (PMMA) as an interacting block during the synthesis of NPs.[30] These observations supported the idea that a similar number of interacting units in the polymer chain would be required to form NPs with similar sizes.

In the case of Au NPs based on PEO-*b*-PAA copolymers, although DHBCs with five different molecular weights (P1–P5) were used, the fixed relative ratio (R = 3) in all NP syntheses resulted in Au NPs of similar size ranges. Thus, instead of the total amount of the carboxylic acid group, the relative molar ratio of interacting units (*i.e.* carboxylate groups in the PAA block in the copolymer to the Au precursor) is regarded as an important factor in determining the size and structure of the resulting Au NPs.

The different amounts of PAA chains used in each Au@DHBC (from Au@P1 to Au@P5), however, can lead to differences in the density of the PEO blocks present on the surface of NPs (Scheme 2). For example, Au@P1 uses a larger number of PAA chains to form a single NP compared to Au@P5 because the $DP_{n,\ AA}$ of P1 is much lower than that of P5. As a result, Au@P1 may have more solvating PEO blocks on the NP surface compared to Au@P5, leading to a higher density of PEO chains on the NP surface.

In order to unambiguously confirm the relative differences in the density of solvating PEO blocks between NPs, Au@DHBC NPs were studied by thermogravimetric analysis (TGA). TGA measurements provide the relative weight contents of Au and DHBC and allow the areal chain density of PEO shells on the surface of Au NPs to be determined (Table 3). For example, Au@P1 had a weight ratio of 29% Au with the volume of a spherical single Au@P1 NP being simply calculated from the radius of the obtained NP. The number of PEO chains on the single NP could therefore be estimated from the volume of single NPs, density of Au (19.3 g cm^{-3}), and molecular weight of the DHBC template ($M_{n,\ NMR}$ of P1 = 9600; see Table 1). Finally, the areal PEO chain density of Au@P1 was evaluated to be 8.4 chains per nm^2 based on the number of PEO chains present on a single NP and the surface area of spherical Au@P1. As the chain length of the interacting PAA blocks increased, it was observed that the relative areal density of the PEO block decreased in the order of Au@P1 > Au@P2 > Au@P3 > Au@P4 > Au@P5.

Based on these results, the PEO shell density on the Au surface may be tuned by controlling the length of the interacting PAA block length. Furthermore, such differences in the

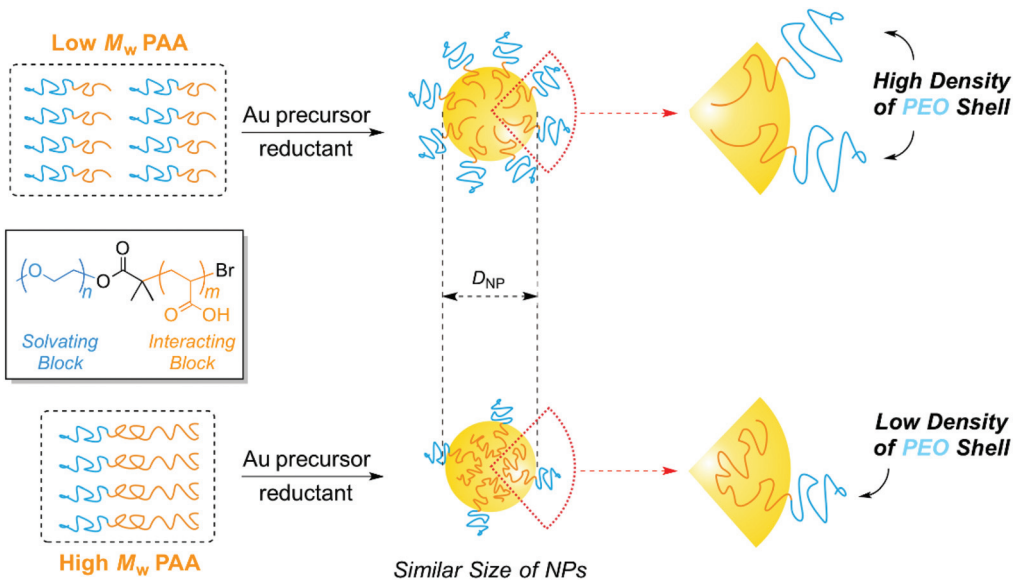

Scheme 2 Schematic representation of changes in Au NP structure that vary depending on the molecular weight of the PAA block in DHBC templates.

Table 3 Thermogravimetric analysis of Au@DHBC NPs and other characteristics

Entry	Weight%[a]			Weight ratio[b]	Radius of Au NP[c] (nm)	Number of PEO chains per NP[d]	Areal density of PEO chain[e] (chains per nm^2)
	Au	DHBC	PEO				
Au@P1	29	71	35	1.2	8.7	7640	8.1
Au@P2	39	61	26	0.7	8.4	3740	4.3
Au@P3	43	57	18	0.4	9.6	3580	3.1
Au@P4	45	55	13	0.3	7.9	1350	1.7
Au@P5	47	53	8	0.2	8.2	950	1.1

[a] The weight% of Au and DHBC were obtained by TGA measurements. [b] The weight ratio of PEO chains to Au can be defined as [weight% of DHBC ÷ weight% of Au]. [c] Radius was calculated by TEM analysis. [d] Number of chains per NP = {[the weight ratio of polymer to Au] × [volume of the spherical Au NP (4/3 × π × Au radius^3)] × [density of Au (19.3 g cm^{-3})] × Avogadro's constant (6.02 × 10^{23})} ÷ (M_w of the DHBC template) (see Table 1). [e] Areal chain density = [number of chains per NP] ÷ [surface area of the spherical Au NP (4 × π × radius of Au NP^2)].

density of the PEO block may allow the overall stability of the Au NP to be controlled. The effect of PEO shell density on the stability of NPs was then evaluated *via* thermal and etching experiments.

The thermal stability of all Au@DHBC NPs at 95 °C was maintained for several days without any noticeable difference between the samples (Fig. S4†). The cyanide etching experiments were also performed on Au@DHBC NPs to clearly demonstrate the effect of the PEO shell density on stability. Au@citrate and Au@P2 NPs were therefore subjected to etching using a dilute cyanide solution (Fig. 5a and b) and, as expected, the Au@citrate sample underwent complete degradation within 30 min with the corresponding surface plasmon band having disappeared rapidly. In direct contrast, Au@P2 NPs exhibited relatively slow degradation in the presence of cyanide ions with only 13% decrease in the surface plasmon band intensity at 520 nm after 30 minutes. Moreover, all Au@DHBC NPs showed a similar etching behaviour with slightly different degradation rates according to their PEO shell density (Fig. 5c). For example, the decrease in plasmon band intensity for Au@P1 with a high PEO shell density was 37%, while the Au@P5 sample with a low PEO shell density showed 52% decrease after 120 min. In a previous report on the stability of NPs against cyanide digestion, it was shown that the higher density of surface ligands serves as a better barrier to prevent the cyanide etching of Au atoms.[24] Similarly, for the Au@DHBC system described in this work, the digestion rate of Au@P1 NPs is directly related to the shell density: the stability increases with increasing chain density of the PEO shell.

Based on the NP synthesis and etching experiments, the effect of the copolymer chain density on colloidal stability is graphically represented in Scheme 3. In Au@DHBC NPs of a similar size, the difference in the density of the PEO shells anchored on the NP is determined by the length of interacting PAA blocks, as described in Scheme 2. This difference results in a relatively condensed surface ligand layer on the Au@P1 NP, which is responsible for the increased steric shielding of the NP surface. In contrast, the Au@P5 NP has a loosely packed surface ligand. A dense polymeric layer of PEO can effectively protect the NP against external chemicals such as cyanide ions and thus facilitate the formation of more stable NPs in solution. Furthermore, this DHBC-based approach enables the synthesis of NPs with stability that can be varied as a function of the molecular weight of interacting blocks.

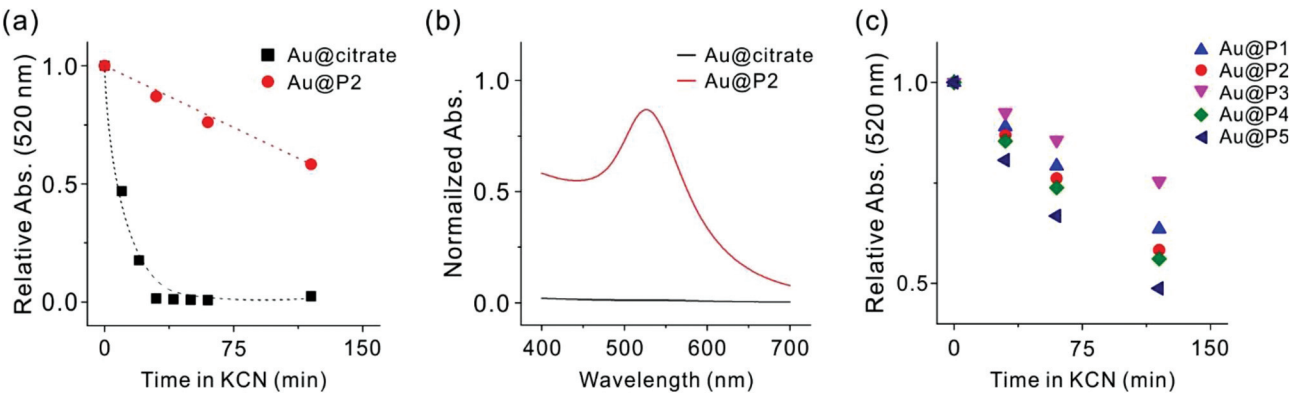

Fig. 5 Cyanide etching of Au NPs in KCN solution (12 mM). (a) Relative absorbance at 520 nm, (b) normalized absorbance after 30 min treatment with Au@citrate (black color) and Au@P2 (red color) NPs. (c) Comparison of relative absorbance changes in different Au@DHBC NPs after treatment with KCN.

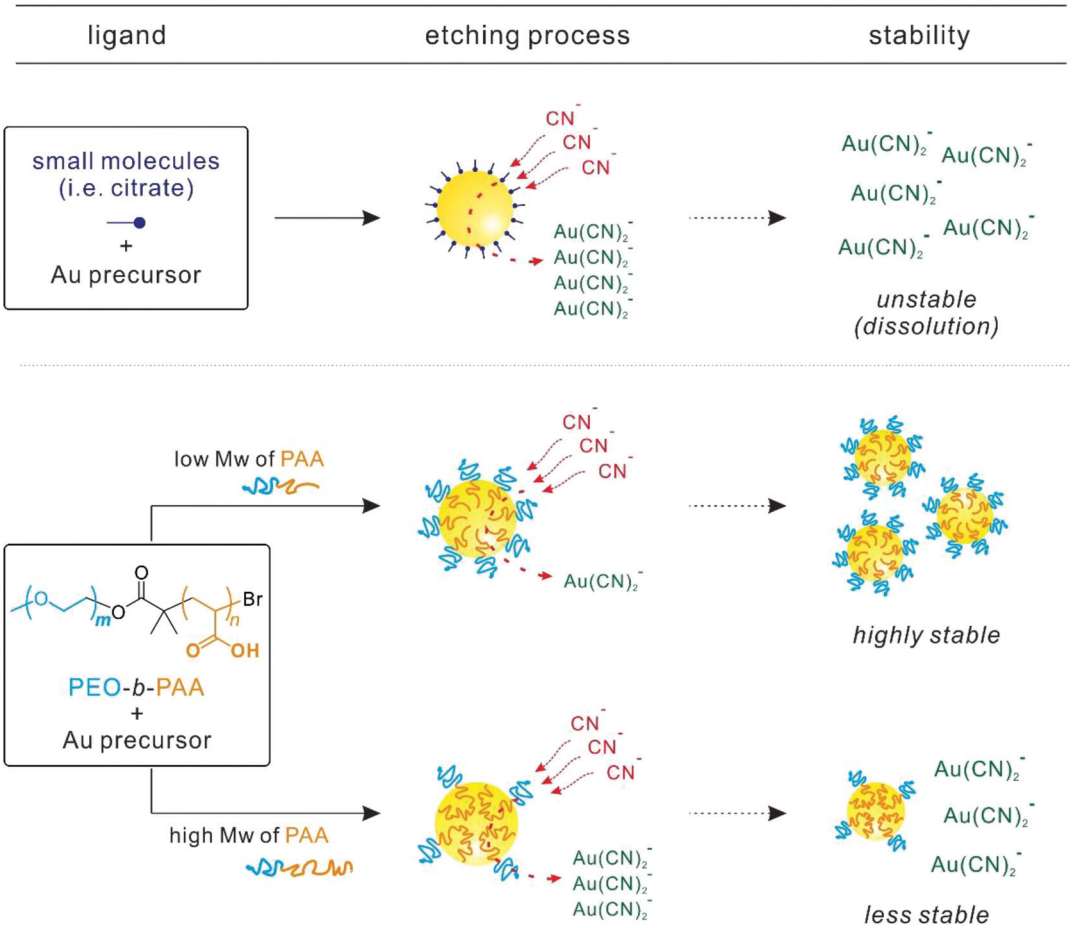

Scheme 3 Schematic representation of Au NPs and their etching performance that vary depending on the molecular weight of the PAA block and the corresponding density of the PEO block on the surface of Au NPs.

Conclusions

In this report, the structural role of double hydrophilic block copolymers (DHBC) in the synthesis of Au nanoparticles (Au NPs) has been investigated. In PEO-*b*-PAA copolymer-based synthesis, it was found that highly stable Au NPs can be formed with the assistance of two chemically distinct blocks: an interacting PAA block to bind with Au ions and a solvating PEO block to sterically stabilize the NPs under harsh conditions (*e.g.*, high temperature, varying pH, and an etching process). Although the molecular weight of the PAA block in the copolymers was not a critical factor for determining the size of NPs, it was found to contribute to the difference in the densities of PEO shells present on the surface of the NPs. This difference allows for the possibility of synthesizing NPs whose stability can be controlled by the molecular weight of the different copolymer blocks. The use of a DHBC having both hydrophilic and biocompatible components for the synthesis of NPs increases potential applications in biomedicine and bioengineering. We expect that the protocol presented in this study will offer a new means for preparing various NPs with superior stability.

Acknowledgements

This work was supported by the National Research Foundation of Korea (NRF-2016 K1A3A1A21005723). Funding is also acknowledged from the Institute for Collaborative Biotechnologies through grant no. W911NF-09-0001 from the U.S. Army Research Office and the use of facilities was supported by the National Science Foundation (Materials Research Laboratory, DMR-1121053). The content of the information does not necessarily reflect the position or the policy of the US government and no official endorsement should be inferred.

Notes and references

1 R. M. Crooks, M. Zhao, L. Sun, V. Chechik and L. K. Yeung, *Acc. Chem. Res.*, 2001, **34**, 181–190.
2 J. Pérez-Juste, I. Pastoriza-Santos, L. M. Liz-Marzán and P. Mulvaney, *Coord. Chem. Rev.*, 2005, **249**, 1870–1901.
3 Y. Xia, Y. Xiong, B. Lim and S. E. Skrabalak, *Angew. Chem., Int. Ed.*, 2009, **48**, 60–103.

4 J. Chen, F. Saeki, B. J. Wiley, H. Cang, M. J. Cobb, Z.-Y. Li, L. Au, H. Zhang, M. B. Kimmey and X. Li, *Nano Lett.*, 2005, **5**, 473–477.
5 M.-C. Daniel and D. Astruc, *Chem. Rev.*, 2004, **104**, 293–346.
6 C.-A. J. Lin, T.-Y. Yang, C.-H. Lee, S. H. Huang, R. A. Sperling, M. Zanella, J. K. Li, J.-L. Shen, H.-H. Wang and H.-I. Yeh, *ACS Nano*, 2009, **3**, 395–401.
7 C. J. Murphy, A. M. Gole, J. W. Stone, P. N. Sisco, A. M. Alkilany, E. C. Goldsmith and S. C. Baxter, *Acc. Chem. Res.*, 2008, **41**, 1721–1730.
8 X. Yang, M. Yang, B. Pang, M. Vara and Y. Xia, *Chem. Rev.*, 2015, **115**, 10410–10488.
9 E. C. Dreaden, A. M. Alkilany, X. Huang, C. J. Murphy and M. A. El-Sayed, *Chem. Soc. Rev.*, 2012, **41**, 2740–2779.
10 N. R. Jana, L. Gearheart and C. J. Murphy, *Langmuir*, 2001, **17**, 6782–6786.
11 T. K. Sau and C. J. Murphy, *J. Am. Chem. Soc.*, 2004, **126**, 8648–8649.
12 K. Kobayashi, J. Wei, R. Iida, K. Ijiro and K. Niikura, *Polym. J.*, 2014, **46**, 460–468.
13 I. Banerjee, R. C. Pangule and R. S. Kane, *Adv. Mater.*, 2011, **23**, 690–718.
14 M. Roberts, M. Bentley and J. Harris, *Adv. Drug Delivery Rev.*, 2012, **64**, 116–127.
15 M. H. Stewart, K. Susumu, B. C. Mei, I. L. Medintz, J. B. Delehanty, J. B. Blanco-Canosa, P. E. Dawson and H. Mattoussi, *J. Am. Chem. Soc.*, 2010, **132**, 9804–9813.
16 Y. Chen, J. Cho, A. Young and T. A. Taton, *Langmuir*, 2007, **23**, 7491–7497.
17 Y. Kang and T. A. Taton, *Macromolecules*, 2005, **38**, 6115–6121.
18 Y. Que, C. Feng, S. Zhang and X. Huang, *J. Phys. Chem. C*, 2015, **119**, 1960–1970.
19 B. P. Bastakoti, S. Guragain, S.-i. Yusa and K. Nakashima, *RSC Adv.*, 2012, **2**, 5938–5940.
20 H. Cölfen, *Macromol. Rapid Commun.*, 2001, **22**, 219–252.
21 K. Nakashima and P. Bahadur, *Adv. Colloid Interface Sci.*, 2006, **123**, 75–96.
22 L. M. Bronstein, S. N. Sidorov, P. M. Valetsky, J. Hartmann, H. Cölfen and M. Antonietti, *Langmuir*, 1999, **15**, 6256–6262.
23 S. N. Sidorov, L. M. Bronstein, P. M. Valetsky, J. Hartmann, H. Cölfen, H. Schnablegger and M. Antonietti, *J. Colloid Interface Sci.*, 1999, **212**, 197–211.
24 B. C. Mei, E. Oh, K. Susumu, D. Farrell, T. Mountziaris and H. Mattoussi, *Langmuir*, 2009, **25**, 10604–10611.
25 F. Bouyer, N. Sanson, M. Destarac and C. Gerardin, *New J. Chem.*, 2006, **30**, 399–408.
26 L. Bronstein, S. Sidorov, A. Gourkova, P. Valetsky, J. Hartmann, M. Breulmann, H. Cölfen and M. Antonietti, *Inorg. Chim. Acta*, 1998, **280**, 348–354.
27 C. Gérardin, N. Sanson, F. Bouyer, F. Fajula, J. L. Putaux, M. Joanicot and T. Chopin, *Angew. Chem., Int. Ed.*, 2003, **42**, 3681–3685.
28 L. Qi, H. Cölfen and M. Antonietti, *Chem. Mater.*, 2000, **12**, 2392–2403.
29 E. Seo, J. Kim, Y. Hong, Y. S. Kim, D. Lee and B.-S. Kim, *J. Phys. Chem. C*, 2013, **117**, 11686–11693.
30 E. S. Cho, F. Qiu and J. J. Urban, *Small*, 2016, 1602572.